39th AIAA/ASME/SAE/ASEE Joint Propulsion Conference & Exhibit
20-23 July 2003, Huntsville, Alabama

AIAA 2003-5153

EXPERIMENTAL STUDY OF ACCELERATION REGION IN A 2 KW HALL THRUSTER

Y. Raitses, D. Staack, L. Dorf and N. J. Fisch
Princeton Plasma Physics Laboratory, Princeton, NJ 08543

ABSTRACT

Measurements with a movable emissive probe in a 2 kW Hall thruster revealed several interesting phenomena. The length of the acceleration region almost does not change when the discharge voltage increases from 200V to 400 V and a growth of maximum electron temperature with the discharge voltage in this range is fairly linear. However, at the discharge voltages above 400 V, the maximum electron temperature saturates at 50 eV, accompanied by a wider acceleration region. These results suggest that the dominant mechanism of the electron mobility is sensitive to the discharge voltage. The role of the secondary electron emission appears to be less important at moderate discharge voltages (less than 400 V in our thruster).

I. INTRODUCTION

In Hall thrusters, a significant voltage drop occurs in the vicinity of the maximum magnetic field near the thruster exit forming the so-called acceleration region (AR). [1,2] In the early 70's Erofeev and Zharinov suggested that the length of the acceleration region (LAR) in Hall thrusters is a self-consistent parameter, which sustains the equilibrium between ionization within the region and diffusion of electrons from the AR to the anode.[2] It was suggested that by controlling the electron mobility and wall losses it is possible to obtain some limiting thruster case with the maximum electric field such as anode layer thruster.[2] For Hall thrusters with ceramic walls, Kim assumed electron wall collisions as dominant mechanism of the electron transport and derived approximate scaling relationship for an efficiency thruster with a constant LAR. This relationship, $\sqrt{V_d}/B_{opt}$ ~constant, couples the discharge voltage, V_d, and some optimal magnetic field, B_{opt}, corresponding to the minimum non-oscillatory discharge current, and the length of the acceleration region.[3] In this case, the electric field is proportional to the discharge voltage, V_d.

Kim's scaling relationship was indirectly confirmed in experiments by measuring integral discharge and ion flux characteristics for different high performance Hall thrusters.[4,5] Hargus and Cappelli conducted direct measurements of plasma parameters in the acceleration region of a laboratory Hall thruster.[6] Using emissive probe and LIF diagnostics they reported no changes of the LAR with the discharge voltage at a constant magnetic field. Similar results were also reported in Ref. 7 using a movable floating probe. However, Kim's scaling is not so applicable to these results measured at low discharge voltages and, therefore, probably with low ionization efficiencies. Most recently, Hofer and Gallimore conducted measurements with a movable floating probe for a high performance Hall thruster at discharge voltages of 300 V and 600 V.[8] Although their results showed also almost no changes in the LAR with the discharge voltage, the floating potential measurements are sensitive to the electron temperature in particular at the low potential edge of the AR, at which energetic electrons from the cathode are injected to the plasma.[9]

Note that for the purpose of scaling, the assumption of the constant LAR in Ref. 3 uses the electron-wall collision frequency proportional to $\sqrt{V_d}$. There have recently appeared a number of theoretical and experimental studies considering the effect of material properties on plasma flow and plasma–wall interaction in a Hall thruster discharge.[10-14] Barall et al. predicted the existence of two different regimes for the electron wall interaction at different discharge voltages. These regimes are associated with the space charge limited sheath at the emitting channel walls. It is reasonable to expect different LAR for different near wall regimes. Ahedo et al.[15] assumed the Bohm diffusion and found that LAR ~ $V_d^{1/4}$. Furthermore, Boeuf with co-workers considered two different anomalous transport mechanisms (Bohm diffusion and electron-wall collisions) and showed that LAR increases with the discharge voltage.[16]

Note that in our previous studies of the segmented electrode Hall thruster a substantial shift of the

acceleration region towards the anode was measured .It was then explained by applying Keidar et al. [10] model of the effect of secondary electron emission on the plasma flow and by considering the effect of the electrode conductivity.[9]

A better understanding of the physical mechanisms, which affect the behavior of the acceleration region and its dependence on the thruster operating conditions, could help to obtain fundamental limitations for scaling of Hall thrusters. In this work we present results of probe measurements of plasma potential and electron temperature in the acceleration region, which are partially consistent with some of these theoretical predictions. The experimental setup is described in Section II. Section III addresses with experimental procedure. Analysis of plasma perturbations induced by probes is also described in this section. Experimental results and their analysis are presented in section IV.

II. EXPERIMENTAL SETUP

The thruster experiments were conducted in the large HTX (Hall Thruster Experiment) vacuum facility consisting of a 28 m^3 vacuum vessel equipped with two CVI cryogenic pumps: a TM 1200i and TMP 1000. The total measured pumping speed is≈62,000 l/s with xenon flow.

A 2 kW Hall thruster (Fig. 1) consists of a coaxial channel made from a boron nitride ceramic material (grade HP), magnetic circuit, and the flat anode, which is also a gas distributor. The outer and inner diameters of the ceramic channel are 123 mm and 73 mm, respectively. The effective channel length taken from the anode to the channel exit is 46 mm. A commercial hollow cathode is used as the cathode-neutralizer.

The flow of xenon gas to the anode and the cathode is controlled by two commercial flow controllers (anode 0-80sccm and cathode 0-10 sccm). To support the thruster operation, a 1kV-10A voltage regulated switching power supply is used. Ref. 9 describes test facility and the thruster design in details.

Diagnostic setup includes fast movable emissive probe, three stationary cylindrical probes mounted near the channel exit and a slow movable probe (emissive and planar biased). The fast movable probe is introduced into the thruster axially through the channel exit. In the present experiments, we used two types of the probe design, conventional unshielded probe and segmented shielded probe. The latter was shown to induce much less plasma disturbances than the unshielded probe. The shield is made from carbon ringlets (Fig. 2) [17]. We found that such segmentation reduces arcing, which could be caused by shorting the plasma by a conductive shield.

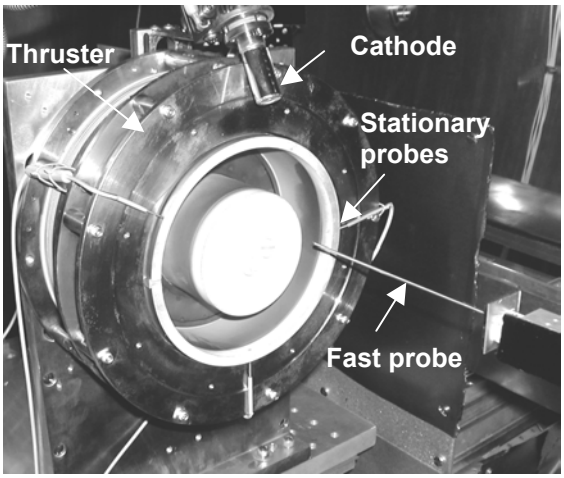

Fig. 1 A 2 kW Hall thruster with probe diagnostics.

The unshielded probe consists of a 1.1 mm diameter double bore alumina tube. The same diameter alumina tube is also used in construction of the shielded probe. Carbon ringlets are glued to the tube with high temperature cement (Fig. 2). The spacing between ringlets is less than 0.5 mm.

The filament is a 0.25 mm diameter thoriated tungsten wire etched at the tip to approximately 0.1 mm diameter, which is several times less than electron gyroradius for operating conditions described in this paper (B_{max}= 150 Gauss, Te > 15 eV). A typical longitudinal size of probe filaments was ~ 2 mm. This probably dictates the minimum spatial resolution of the probe along its path across the magnetic field.

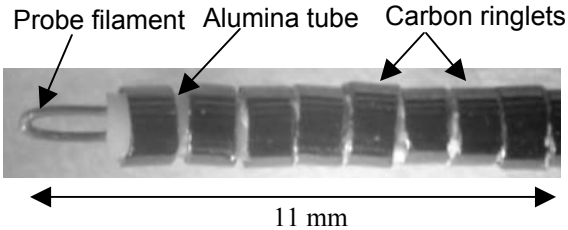

Fig. 2 Emissive probe with segmented shield made from carbon ringlets.

The emissive probe with electrical connections and wires is assembled on an aluminum probe arm, which is fixed on the fast positioner through an adjustable stage (Fig. 3). The arm is covered with a carbon velvet plate in order to prevent it from sputtering caused by energetic ions of the plasma jet during probe measurements. The fast positioner, which is described in details in Ref. 9, is capable of up to 12 g's acceleration with a maximum load of 3 Kg. The encoder resolution is 0.01 mm, and the maximum speed

is 1500 mm/s. The positioner is mounted on a X-Y movable table (Fig. 3).

All electrical connections in the probe circuits are from vacuum side protected from leakage current. The floating potential of the emissive probe is measured relative to ground by using a 100:1 divider (500 MOhm :5 MOhm) connected to a high input impedance isolation amplifier.

The stationary cylindrical probes are used to monitor changes in the thruster operation and plasma perturbations induced by the fast probe relative. The slow movable biased and emissive probes are used to measure the plasma parameters in the near anode region, in which fast probe measurements can disturb the plasma.[18]

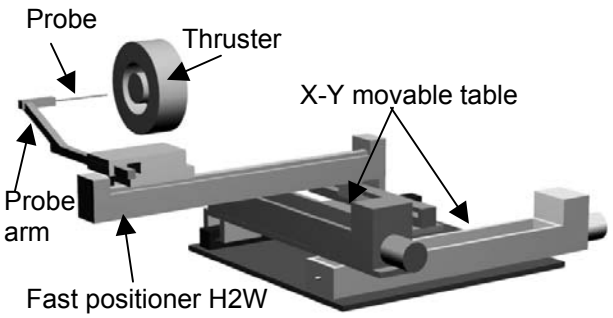

Fig. 3 A schematic of the fast movable probe and positioning system. The initial placement of the probe tip is 250 mm from the channel exit.

The data acquisition system (National Instrument PCI-6071E board) was configured to measure probe potentials, heating power, cathode potential relative to ground discharge current and probe position at 10 kHz acquisition rate when triggered by a digital signal from the fast positioner controller at the beginning of motion.

III. EXPERIMENTAL PROCEDURE

Thruster operation

The thruster was operated at two anode mass flow rates of xenon gas (research grade), 3 mg/sec and 5 mg/sec. The cathode flow was kept constant, 0.2 mg/s, for all operating regimes. The discharge voltage range was 200-600 V. The magnetic field was kept constant throughout these experiments. Fig. 4 shows results of non-linear simulations of the magnetic field distribution. The channel exit is 46 mm on these plots. Simulations were conducted using measured B-H curve of the low carbon steel used in the thruster design. A comparison of simulated and measured results showed a very good agreement.

The shape of the magnetic field distribution is different from what is typically used in conventional Hall thrusters. The number of ampere-turns was larger in the inner coil than in the outer coil leading to a mirror at the inner wall. We found that the thruster operation with such magnetic field distribution is less likely be perturbed by the fast probe measurements.

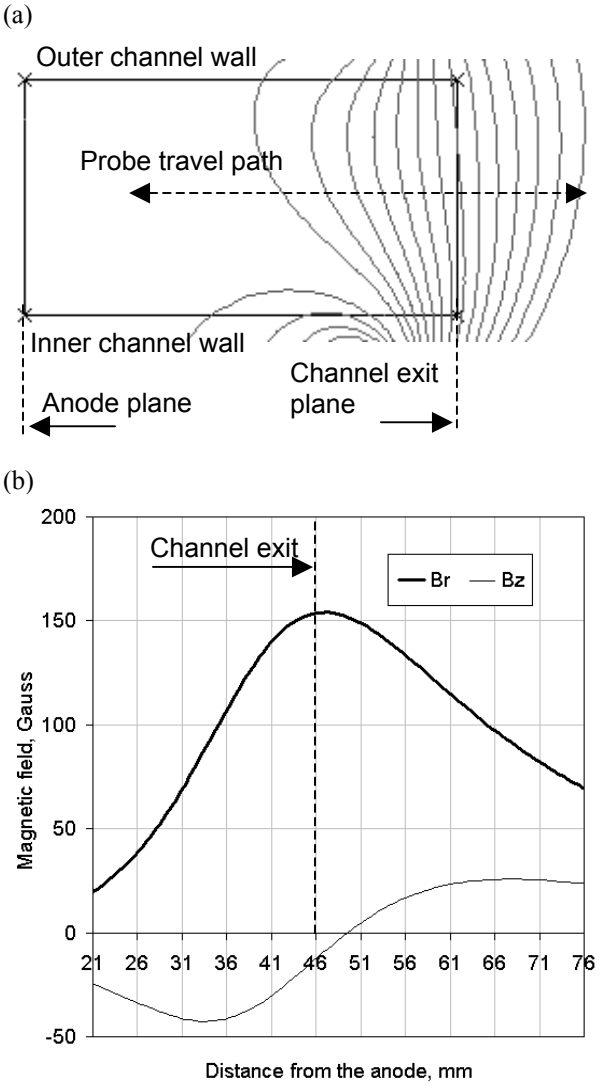

Fig. 4 Magnetic field distribution: flux lines (a) and profiles of radial and axial components of the magnetic field (b), B_r and B_z, respectively, along the channel median (a probe travel path). The channel exit is at 46 mm.

In all the experiments described in this paper, the same thruster channel and anode were used without removal of dielectric coatings, which were typically observed, in particular on the channel interior surface.

Probe measurements

Probe measurements were conducted in three separate sets of experiments with three probes of two different types, namely, segmented shielded probe, referred in this paper as SP, and two identical unshielded probes referred as AP1 and AP2. Measurements at 3 mg/s were conducted essentially with the AP1 probe and, in some regimes, with the AP2 probe. Each probe was used in measurements at 5 mg/s. The main reason for using different probes in these experiments is related to typical contaminations of alumina tubes and modifications of alumina material caused probably by overheating and frequent exposure to the plasma jet. The same issue is relevant for the shielded probe.

At the beginning of each set of experiments, the thruster was allowed continuous operation for approximately 1-2 hours, in order to reach a steady state. Then, the thruster was turned off for about 30-40 minutes, while the X-Y table placed the fast positioner with the probe to the initial radial placement in front of the thruster at the channel median (Fig. 3). Note, that the probe alignment was conducted before each set of experiments using the inner and outer channel walls as the references.

After the probe was placed at the initial position, the thruster was operated again for about 30 minutes before beginning of a set of measurements was initiated. In each operating regime of the thruster floating potential measurements were conducted first without the heating (cold probe) and then with heating on (hot probe). Probe heating was gradually increased during several probe insertions until the floating potential clearly saturated along the travel path of the probe. Measurements with cold and saturated hot probe were repeated 2-4 times in most of the operating regimes, in particular in those with relatively large probe-induced perturbations.

The measured data (probe and cathode potentials, discharge current) from multiple probe insertions, including probe motion on its way in and out were binned and averaged at 0.2 mm spacing to reduce the signal to noise ratio and then smoothed by adjacent averaging with a step of ± 1.6mm. The number of points binned varied from 16 to 100 depending on the probe speed, travel distance, motion sequence and number of data files averaged. Fig. 5 shows smoothed floating potential profiles for the hot SP probe and standard deviation (STDV) of the raw data. In general, for all three probes, larger spread of the measured results (± 30-35%) took place in operating regimes with larger discharge voltages (≥400V). Probe-induced perturbations of the plasma caused stronger irreproducibility of the measurements. For example, the increase of STDV seen in Fig. 5b near the thruster exit coincides with probe perturbations. In addition, the oscillations could cause larger deviations of the signal measured in the plume due to smaller signal-to-noise ratio. At moderate discharge voltages deviations were less than ± 15% for the shielded and unshielded probes.

(a)

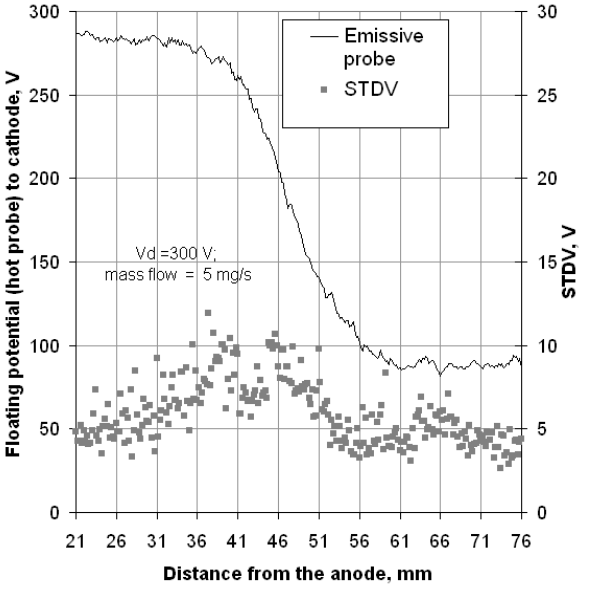

(b)

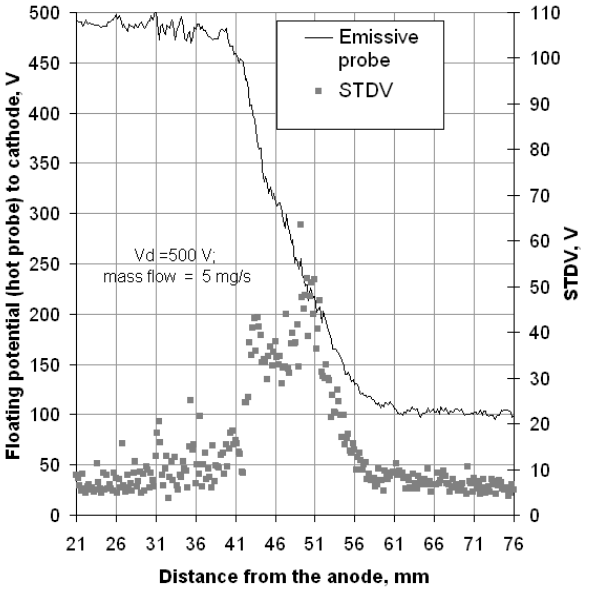

Fig. 5 Floating potential of the emissive SP probe relative to cathode along the channel median and STDV of the measurements for two operating regimes at 300 V and 500 V. The anode flow rate is 5 mg/s. Channel exit is 46 mm. The data is averaged with spacing 0.2 mm.

Determination of plasma parameters

Floating potentials relative to the cathode were estimated for each probe insertion. Uncertainties due to the potential drop across the probe filament were assumed equal to a half heater voltage ~ 6V are included in estimations of the hot probe potential.

The plasma potential and the electron temperature were deduced from hot and cold probe measurements like in Ref. 19, but taking into account the potential drop in the sheath and pre-sheath formed between the probe surface and the plasma.

The emitted electrons from the hot floating probe are much colder than plasma electrons collected by the probe. In the case of strong electron emission, a double layer is formed near the surface of the filament, restricting flux of emitted electrons.[20] As a result, the voltage drop between the plasma and the hot floating probe eventually saturates as the probe temperature increases.

Following Schwager[21], we can obtain an approximate relation between the plasma potential, ϕ_{pl}, and the floating potential of a hot probe ϕ_{fl}^{em}, which for Xenon plasma becomes

$$\phi_{pl} = \phi_f^{em} + 1.5 \cdot T_e \qquad (1)$$

Assuming Maxwellian electron distribution function (EDF) and neglecting flux of energetic ions to the probe, we can use the classical expressions for the difference between the plasma potential and the floating potential of a cold probe, ϕ_f^{cl}, which for Xenon plasma is

$$\phi_f^{cl} = \phi_{pl} - 5.77 \cdot T_e , \qquad (2)$$

where T_e is the electron temperature. Since the thickness of a near-probe pre-sheath in Hall thruster plasma can be comparable with the channel height[10], it is reasonable to suggest that a floating emissive probe measures values of the plasma potential and electron temperature averaged over the channel height. Thus, the probe resolution in the radial direction is assumed to be equal to the channel height 25 mm and in the axial direction it is assumed to be equal to the probe longitudinal size ~ 2mm.

From Eqs. (1) and (2), the electron temperature can be obtained in a form,

$$T_e = \frac{\phi_f^{em} - \phi_f^{cl}}{4.27} . \qquad (3)$$

Note that Eq (3) has two measured parameters. The calculated electron temperature is then substituted in Eq. (1) to account for the sheath-pre-sheath effects in estimations of the plasma potential.

In spite of simplicity of the data analysis and certain other advantages of using non-biased emissive probes in Hall thrusters, the assumption of the Maxwellian EDF introduces significant uncertainty in determination of the electron temperature (Eq. (3)). A number of theoretical studies suggest that the electron distribution function in Hall thrusters is generally non-Maxwellian.[22] Latocha et al. showed some cases when Maxwellian EDF may still be applicable by forcing the mean electron energy to be equal to one determined from the proposed non-Maxwellian EDF. Other probe techniques used in Hall thruster studies elsewhere, including biased movable and stationary probes[23], cylindrical, flat, double and hot floating emissive probes[24], give comparable results and profiles for similar thrusters and operating conditions. It seems, therefore, that the electron temperature defined by Eq. (3) is essentially the mean electron energy for Hall thruster plasma.

Without considering basic issues discussed above, the uncertainty in determination of the electron temperature was estimated for each probe type as the sum of deviations of the hot probe and cold probe. The electric field was calculated by differentiating the plasma potential distribution, smoothed over ± 2.5 mm, in order to reduce numerical noise.

IV. EXPERIMENTAL RESULTS & DISCUSSIONS

Discharge characteristics

Fig. 6 compares the voltage versus current characteristics measured for the thruster with two types of the magnetic field distribution. In general, these characteristics are comparable, particularly for the small flow rate. Note that the discharge voltage of 400 V is some sort of threshold above which an increase of the discharge current becomes noticeable. Gascon et al. measured a similar behavior for SPT-100ML thruster and found it common for different ceramic channel materials.[13] We will return to this interesting behavior in analysis of our plasma measurements.

For both modified and conventional magnetic field configurations we measured comparable propellant and current utilization efficiencies ~ 0.9 and 0.8, respectively, though the plume angle was larger (by 5°-10°) in the present configuration. From these measurements it appears that the thruster operation in the present configuration, with an unusual shape of the magnetic field distribution, exhibits behavior typical for conventional Hall thrusters.

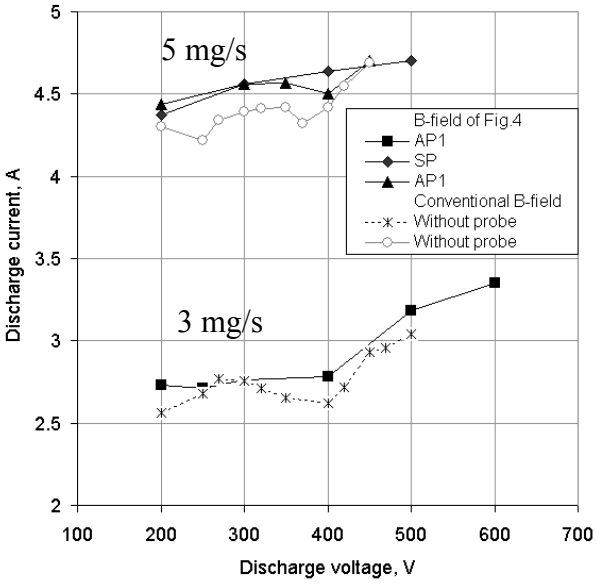

Fig. 6 Discharge characteristics measured for the two types of magnetic field distribution.

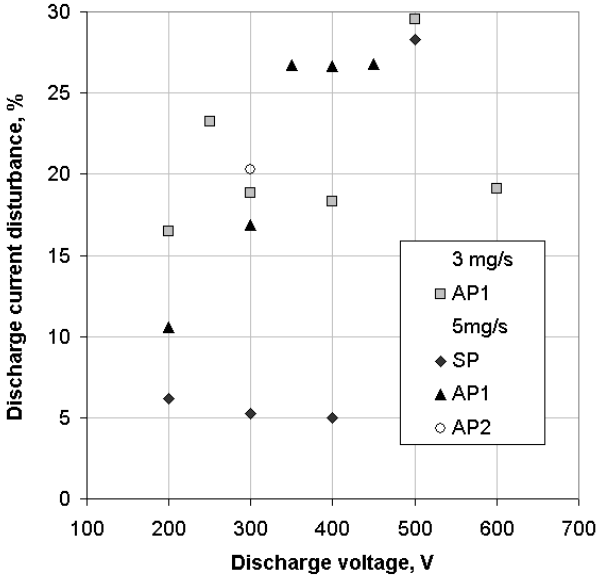

Fig. 7 Relative amplitude of discharge current perturbations for shielded, SP, and unshielded probes, AP1 and AP2.

Probe-induced perturbations

The effect of the movable probes on the thruster plasma was characterized by measurements of the discharge current, stationary probes floating potential, and cathode potential to ground. For the unshielded probes, perturbations of the discharge current start outside of the channel at 5-10 mm from the channel exit. In the case of the shielded probe perturbations are typically observed when the probe passes the channel exit while moving towards the anode, or even deeper inside the channel. Results of Fig. 7 suggest that perturbations of the discharge current were substantially less for the shielded type probe.

At 500 V the shielded probe perturbs the discharge current similar to the unshielded probe. The discharge current reaches about 30% greater than its steady state value, for both probes.

Fig. 8 shows plasma potential profiles for 300 V and 5 mg/s measured with the SP and AP1 probes. These profiles are similar for both probe cases.

Note that plasma perturbations measured with the stationary probe are different for the shielded and unshielded probes. The SP probe induces very small perturbations as compared to the unshielded probe. An increase of the floating potential in the AP case coincides with lower electron temperatures measured by the AP probes (Fig. 9). In other words, the floating potential of the cold probe was larger in the AP1 case than in the SP case. Since perturbations caused by cold and hot probes may occur at different locations, this might cause the shift of the maximum electron temperature, which is seen in Fig. 8.

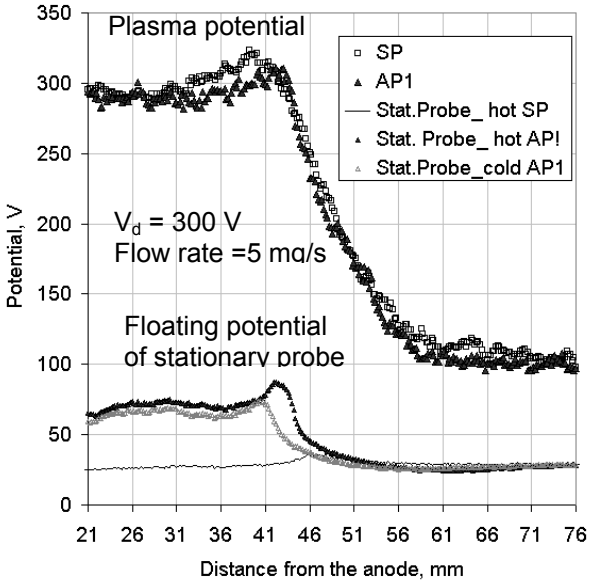

Fig. 8 Plasma potential profiles measured with the AP1 and SP movable probes along the thruster median for the thruster operating at the discharge voltage of 300 V and mass flow rate of 5 mg/s. Floating potential of the stationary probe was simultaneously measured with the hot and cold movable probes. Channel exit is at 46 mm. The data is averaged with spacing 0.2 mm

It was suggested in Ref. 17 that a high secondary electron emission of the probe tube is likely to be the

cause of probe-induced perturbations in Hall thrusters. This is partially consistent with the present results.

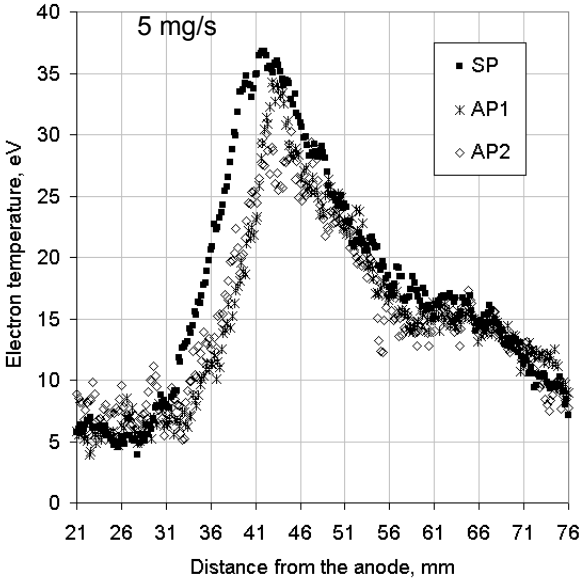

Fig. 9 The electron temperature measured along the channel median with three different probes unshielded AP1 and AP2 probes and shielded SP probe for the discharge voltage of 300 V and mass flow rate 5 mg/sec. Channel exit is 46 mm. The data is averaged with spacing 0.2 mm.

Plasma measurements

Fig. 10 compares plasma potential distributions measured for different voltages and two mass flow rates. Illustrative profiles of the electron temperature are shown in Fig. 11. All profiles are smoothed with a spacing of ± 1.6mm by adjacent averaging. For comparison, non-smoothed profiles, which are simply averaged with a spacing of 0.2 mm, are shown for 500 V and 600 V. The acceleration region with a sharp potential drop can be clearly distinguished from the almost flat potential profile in the plume and from the unusually shaped profiles in the near anode region.

Interestingly, the plasma potential profiles in the near-anode region lie below the anode potential at low discharge voltages (< ~300 V) and above the anode potential at large discharge voltages. This result indicates that the anode sheath changes with the discharge voltage from a positive electron-attracting sheath to a negative, electron-repelling sheath. The transition to the negative sheath regime coincides with the increase of the electron temperature in the near anode region, i.e. the increase electron thermal flux towards the anode (Fig. 11). Similar behavior was also measured with low-disturbing biased and emissive probes.[18] Although it is also expected theoretically that the anode sheath is a function of thruster operating conditions,[25] this relationship is complex and depends also on the thruster configuration. In fact, for a different thruster configuration we obtained a quite opposite result: the negative sheath was measured at low and moderate discharge voltages. Analysis of these interesting phenomena is described in Ref. 26.

(a)

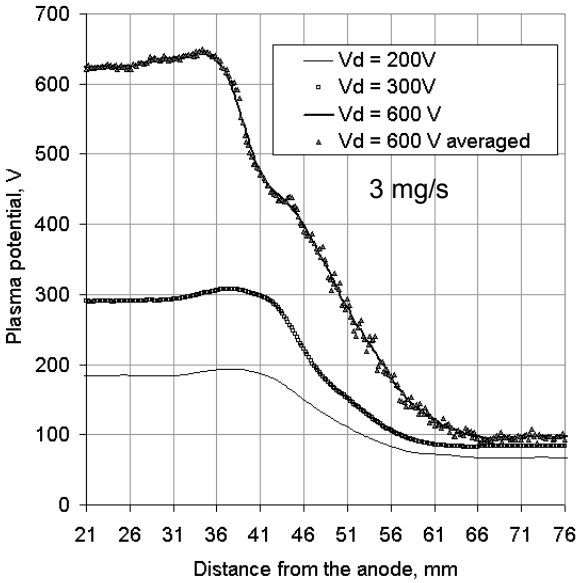

(b)

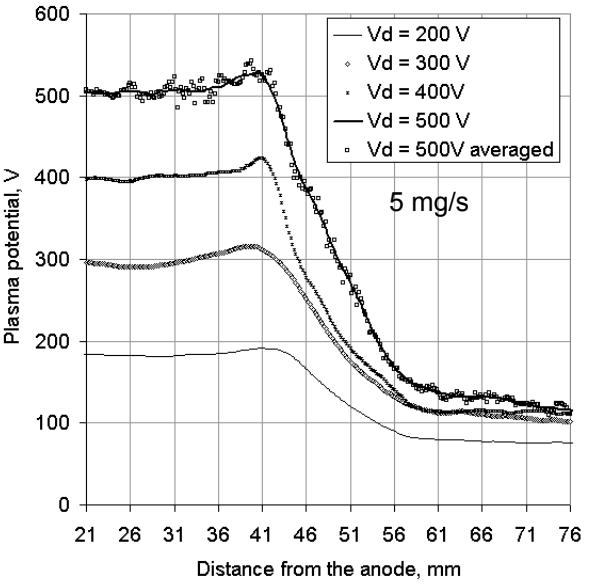

Fig. 10 Plasma potential distribution measured along the thruster median for two flow rates: 3 mg/sec (a) and 5 mg/sec (b). Channel exit is 46 mm. The averaged (0.2 mm) non-smoothed data is shown for comparison with smoothed profiles (± 1.6mm).

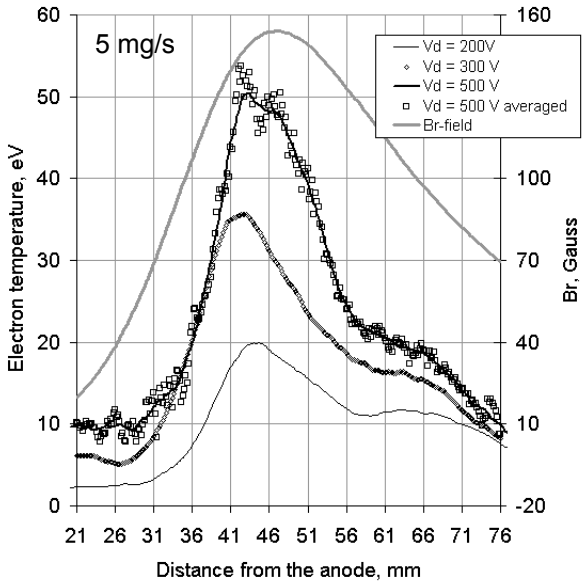

Fig. 11 Electron temperature measured along the thruster median for flow rate of 5 mg/sec (b). Channel exit is 46 mm. The averaged (0.2 mm) non-smoothed data is shown for comparison with smoothed profiles (± 1.6mm).

Parameters of the acceleration region

Fig. 12 shows the maximum electron temperature at different discharge voltages. The increase of the maximum temperature with the discharge voltage is fairly linear up to the discharge voltage of 400 V. A linear fit gives $Te_{max} \propto 0.13V_d$ in this discharge voltage range. Ahedo et al. used a one-dimensional model with thermal conductivity and obtained $Te_{max} \propto 0.2V_d$. It seems that in this discharge voltage range wall losses are insignificant.

At larger discharge voltages, the electron temperature saturates and reaches ~ 50 eV. This behavior appears to be consistent with predictions for the charge-saturated sheath regime, which occurs due to strong secondary electron emission from ceramic walls of the thruster channel. Interestingly, Dawson reported that the first secondary electron emission threshold for a boron nitride ceramic is also at 50 eV.

The observed saturation of the maximum electron temperature is accompanied by the increase of the discharge current (Fig.6). This behavior appears to be consistent with the Barral et al model, which predicts an increase of the electron transport in a space charge saturated sheath regime due to electron-wall collisions. This model would suggest that in our experiments the electron mobility is changed above the threshold voltage of 400 V.

The placement of the acceleration region was estimated for 90% of the voltage drop between the point on the anode side of AR, where the plasma potential is maximum, and the point on the cathode side of AR, where the electric field is equal or close to 0.

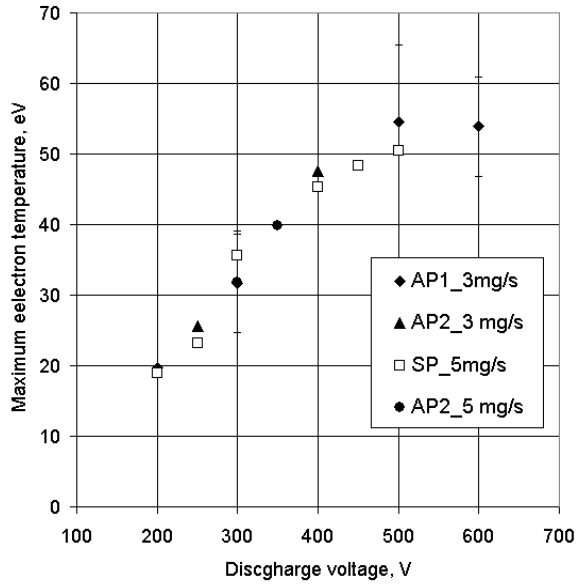

Fig. 12 Maximum electron temperature deduced from the plasma potential measurements along the thruster median at two mass flow rates by 3 different probes and

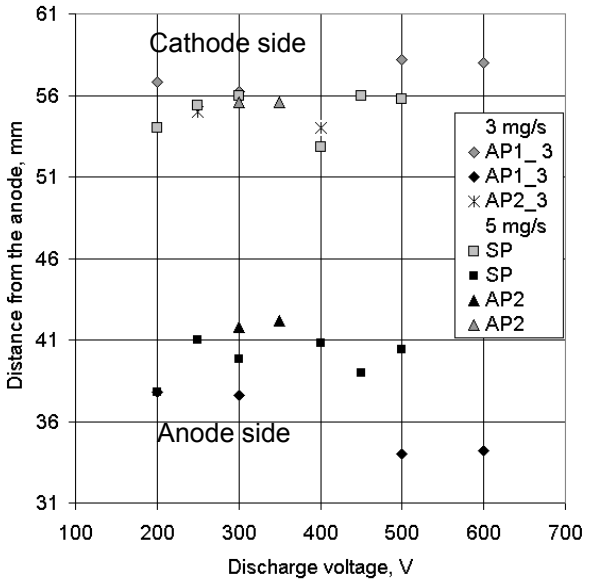

Fig. 13. The placement of the acceleration region estimated for 90% of the voltage potential drop.

Since the potential outside this region changes insignificant, the use of 90% of this voltage drop is a good measure of the region boundaries. In this case, the estimated length includes both ionization and

acceleration regions. As can be seen, there are some correlation between the saturation of the electron temperature and the increase of the discharge current and expansion of the acceleration region at the small flow rate. The region expands towards both the anode and plume when the discharge voltage is larger than 400 V. A larger expansion towards the anode could be also explained by shifting of the ionization region in the case of a negative anode sheath regime.[27] Note that there are almost no changes in the LAR at 5 mg/s, at which the ionization efficiency is higher than at smaller flow rates.

In the regime of a linear dependence of the electron temperature on the discharge voltage, the length of acceleration region almost does not change with the discharge voltage. However, it could be also a result of insufficient axial resolution of this probe. For example, if $L \propto V_d^{1/4}$ (See Ref. 15) then changes in the acceleration region in the discharge voltage range of 200V-400V are expected to be smaller than the axial resolution of the probe (±2mm).

SUMMARY

A discharge voltage threshold has been observed in a laboratory Hall current plasma thruster. This threshold separates two different plasma regimes of the thruster. Below this threshold, which in our experiments was 400 V, the length of the closed electron drift region is insensitive to the voltage but the maximum electron temperature increases linearly with the voltage. Above this threshold, the electron temperature saturates and the drift region expands. This behavior at high discharge voltages appears consistent with predictions of the charge-saturated sheath regime due to strong secondary electron emission from ceramic walls of the thruster channel. The dominant mechanisms of the electron mobility and electron energy losses are likely different in these two regimes. For example, a role of the secondary electron emission appears to be less important below the measured threshold.

ACKNOWLEDGMENT

The authors would like to thank Mr. Artem Smirnov and Dr. Alexander Dunaevsky for fruitful discussions. This work was supported by the US DOE and the NJ Commission on Science and Technology.

REFERENCES

1. S. D. Grishin, V. S. Erofeev, A. V. Zharinov, in the “Plazmennye Uskoriteli”, edited by L. A. Arzimovich, “Mashinostroenie” , Moscow (1973) (in Russian).
2. A. I. Morozov and V. V Savelyev, in the “Reviews of Plasma physics”, edited by B. B. Kadomtsev and V. D. Shafranov, vol. 21, Kluwer Academic Publishers (2000).
3. V. Kim, J. Prop. Power, 14, 726 (1998).
4. D. Manzella, D. Jacobson, R. Jankovsky, AIAA Paper No. 2001-3774, 37-th Joint Propulsion Conference and Exhibit, Salt Lake City, UT.
5. Y. Raitses, J. Ashkenazy, G. Appelbaum, AIAA Paper No. 1998-3640, 34-th Joint Propulsion Conference and Exhibit, July 13-15, 1998, Cleveland, OH.
6. W. A. Hargus Jr., M. A. Cappelli, AIAA Paper No. 1999-2721, 35-th Joint Propulsion Conference and Exhibit, June 20-24, 1999, Los Angeles, CA.
7. Y. Raitses, J. Ashkenazy, in the Proceedings of the XVII-th International Symposium on Discharges and Electrical Insulation in Vacuum, July 1996, Berkeley, CA.
8. R. Hofer, A. Gallimore, IEPC Paper 2003-037, 28-th International Electric Propulsion Conference, March 2003, Toulouse, France.
9. Y. Raitses, D. Staack, A. Dunaevsky, L. Dorf and N. J. Fisch. IEPC Paper 03-0139, 28-th International Electric Propulsion Conference, March 2003, Toulouse, France.
10. M. Keidar, I. Boyd, I. Beilis, Phys. Plasmas 8, 5315 (2001).
11. S. Barral, K. Makowski, Z. Peradzynski, N. Gascon, M. Dudeck, , accepted for publication in Phys. Plasmas (2003).
12. E. Ahedo, Phys. Plasmas 9, 4340 (2002).
13. N. Gascon, M. Dudeck, S. Barral, accepted for publication in Phys. Plasmas (2003).
14. L. Jolivet, J.-F. Roussel, “Effects of the secondary electron emission on the sheath phenomenon in a Hall thruster”, EUSPC.
15. E. Ahedo, J. M. Gallardo, M Martinez-Sanchez, Phys. Plasmas 9 (2002).
16. G. J. M. Hagelaar, J. Bareilles, L. Garrigues, J.-P. Boeuf, J. Appl. Phys. 93, 67 (2003).
17. D. Staack, Y. Raitses and N. J. Fisch, submitted for publication in Rev. Sci. Inst. June 2003
18. L. Dorf, Y. Raitses, N. J. Fisch, to be submitted for publication in Rev. Sci. Inst. in 2003.
19. N. Meezan, W. Hargus Jr., M. Cappelli, Phys. Rev. E 63, Art. No. 026410 (2001).
20. G. D. Hobbs, J. A. Wesson, Plasma Phys. 9, 85 (1967).
21. L. A. Shwager, Phys. Fluids B 5, 631 (1993).

22. V. Latocha, L. Garrigues, P. Degond, J.-P. Boeuf, Plasma Sources Sci. Technol. 11, 104 (2002).
23. G. Guerrini, C. Michaut, M. Dudeck, A. N. Vesselovzorov, M. Bacal, IEPC Paper 97-053, 25-th International Electric Propulsion Conference, Aug. 24-28, 1997, Cleveland, OH.
24. J. Haas, A. Gallimore, Phys. Plasmas 8, 652 (2001).
25. L. Dorf, V. Semenov, Y. Raitses, N. J. Fisch, AIAA paper No. 2002-4246, 38th Joint Propulsion Conference and Exhibit, July 7–10 2002, Indianapolis, Indiana.
26. L. Dorf, Y. Raitses, N. J. Fisch, APS/DPP Meeting, 2003, to be submitted.
27. A. Cohen-Zur, A. Fruchtman, J. Asheknazy and A. Gany, Phys. Plasmas, 9 (2002).